Journal of the European Ceramic Society 20 (2000) 1439–1452

Fracture toughness, strength and thermal shock behaviour of bulk plasma sprayed alumina — effects of heat treatment

R.J. Damani, D. Rubeša, R. Danzer *

Department of Structural and Functional Ceramics, University of Leoben, A-8700 Leoben, Austria

Received 15 February 1999; received in revised form 24 January 2000; accepted 30 January 2000

Abstract

Bulk plasma spraying Al_2O_3 produces a material with a defect rich splat-internal microstructure and a non-equilibrium phase composition which are both subject to extensive change by heat treatment. In the present work heat treatment induced changes in the strength, fracture and thermoshock characteristics of this material have been investigated and related to microstructural development. It is found that the as-sprayed intrasplat defect structure provides low energy paths for crack propagation. This results in low toughness and strength but excellent thermoshock resistance. Heat treatment increases overall porosity, but heals the defect structure and increases splat integrity, leading to a large increase in strength, accentuated *R*-curve behaviour and a disproportionate increase in toughness, but also a reduction in thermoshock resistance.

Keywords: Al_2O_3; Mechanical properties; Microstructure-final; Plasma spraying; Thermal shock resistance

1. Introduction

Plasma spraying provides an economically viable way of producing ceramic components where production by conventional routes would be expensive or restricted due to post-processing or size. Typical products range from large pipes and transport rollers for operation at high temperatures to smaller fibre guides and sleeves for wear resistance. Deposit thickness can be varied from several micrometres for coatings to tens of millimetres for free-standing components. Both coatings and free-standing components can have excellent mechanical properties such as high damage tolerance and thermal shock resistance.[1–4]

Earlier works on plasma-sprayed materials have largely concentrated on coatings. However, a considerable body of empirical work has built up on bulk sprayed material over time. In an early work, Lutz[5] described the elastic response, strength, fracture and thermoshock behaviour of several plasma-sprayed ceramic systems, including alumina, in the as-sprayed and annealed (post-sintered) states. Although very low strength values were reported, their fracture resistance and thermoshock resistance was exeptionally good. However, all the plasma-sprayed materials exhibited considerable anisotropy in their mechanical response, see e.g. Refs. 6 and 7, and in a subsequent work, it was found that the thermoshock resistance of plasma-sprayed ceramics is subject to some sample size dependence.[8] Moreover, strength and fracture resistance could be significantly increased by the post-sintering heat treatments.[9] In a more recent work,[10] it has been shown that the stiffness of bulk plasma-sprayed deposits also exhibits considerable anisotropy and elastic constants are also subject to significant change and eventual increase upon heat treatment. As these works are largely empirical, however, few clear and fundamental mechanistic explanations of the observed behaviour are given, although several inspired suggestions are made.

Clearly, the properties of plasma sprayed ceramics, and especially the differences to properties of conventionally sintered ceramics, can be traced back to their porous, anisotropic, layered *splat* microstructures, which are a consequence of the deposition process.[11,12] Furthermore, as-sprayed ceramic systems are frequently deposited as mixtures of stable and metastable phases.[13–16] It is known that subsequent thermo-mechanical loading can lead to extensive changes in the

* Corresponding author. Tel.: +43-3842-4029100; fax: +43-3842-4029102.

E-mail address: isft@unileoben.ac.at (R. Danzer).

0955-2219/00/$ - see front matter
PII: S0955-2219(00)00033-9

microstructures, and hence properties, of the deposited ceramic.[17–19] Thus, after spraying, components are often subjected to heat treatments to aid homogenisation of the phase system and reduce porosity. Such treatments are particularly common in the alumina system where plasma spraying is known to result in the simultaneous deposition of several metastable transition phases, viz. γ, δ and θ-Al_2O_3. These must go through a thermally activated reconstructive transformation to become thermodynamically stable α-Al_2O_3. However, the heat treatments applied in industry are usually arbitrarily chosen to simply achieve a material with thermal stability or induce apparent post-deposition sintering.

An understanding of the relationships between changes in microstructure resulting from heat treatment and the related effects on properties would facilitate the ability to engineer plasma-sprayed ceramics with different property–microstructure configurations. For instance, in Ref. 9 it was noticed that, contrary to expectation, fracture in as-sprayed material was largely transgranular, through fractured splats, whereas that in material heat treated for 4 h at 1550°C, to convert the material to α-Al_2O_3 and induce splat sintering, occurred mainly intergranularly, involving delamination along intersplat interfaces. It was suggested that a splat internal substructure in the as-sprayed material provided weak paths for crack propagation, and that annealing caused healing of these pre-existing easy crack paths, thereby forcing crack deviation. These weak crack paths were thought to arise for a number of reasons: internal grain structure, impact damage and thermal (quench) cracks.

In a complementary work to this[20] the evolution of the microstructure and substructure of a bulk plasma-sprayed alumina with heat treatment have been systematically investigated. It is the objective of the present work to achieve a clear mechanistic understanding of the thermomechanical behaviour of the same alumina material by investigating its fracture behaviour, strength, and thermoshock resistance as this changes with heat treatment and relating changes to the accompanying development of the microstructure.

2. Material evaluation and experimental procedure

2.1. Material and microstructure

The alumina material used in this investigation was atmospheric plasma spray (APS) deposited by LWK Plasmakeramik, Gummersbach, Germany, using a water stabilised arc plasma gun. It was sprayed from a powder agglomerate (Alcoa CT100, 99.5% α-alumina, with individual crystallite size between 2 and 5 μm) onto a removable steel mandrel in a series of sets of passes, between which the material was allowed to cool to reduce thermal stresses. The ceramic cylinder produced had a wall thickness of about 80 mm. The as-sprayed material had a porosity of about 13%.[20] All samples were cut from the bulk to avoid substrate influence, e.g. substrate-deposit cooling effects.

Heat treatments were carried out with a hold time of 12 h at 900, 1050, 1180 and 1550°C. These temperatures were chosen on the basis of the transformation temperatures for the various metastable alumina phases given in literature.[21,22] The last heat treatment is just below a common sintering temperature for alumina materials,[23] and is similar to treatments applied in industry to consolidate and make thermally stable sprayed products. The samples were heated in air at 5°C/min and furnace cooled to RT.

X-ray phase analysis, transmission electron microscopy (TEM), scanning electron microscopy (SEM), optical microscopy, fractography and Archimedean porosimetry were conducted to characterize material development. Details of the techniques applied may be found in Refs. 9 and 20.

2.2. Evaluation of fracture and thermoshock characteristics

Fracture characteristics were investigated in situ on compact tension (CT) samples in a Leica Cambridge stereoscan 440 SEM using a purpose-built displacement controlled loading device.[24] The samples were prepared with a machined notch cut perpendicular to the splat layers, which was then manually sharpened using a razor blade to a notch tip diameter of about 100 μm in order to minimise notch width influence.[25,26] The samples were sputtered on one side with a fairly thick gold coating before testing. Crack propagation caused this coating to crack, and the crack flanks accumulated charge giving rise to contrast and allowing the in situ observation of crack progress. (Unfortunately this can also have the effect of diminishing the quality of the image observed or recorded.) Sample dimensions and splat orientation may be seen in Fig. 1a. Fracture toughness, K_{Ic}, was evaluated from load and respective crack length a according to $K_{Ic} = Y\sigma a^{1/2}$, where σ is applied stress and Y is the geometric correction factor, as given in Ref. 27.

Thermoshock tests were conducted using standard small beam samples ($3\times4\times45$ mm^3) cut so that the splats lay in a plane parallel to the tensile surface of the beam, Fig. 1b. The edges of the tensile surface were chamfered at 45°. However, because of the cracked nature of the microstructure it was not felt necessary to polish the tensile surface. The samples were held in a magazine and heated in a vertical cylinder furnace at 5°C/min until test temperature was reached. They were then dropped about 50 cm into a sieve in cold water. A mixer was used to keep the water continuously

circulating to reduce the insulating effects of vapour layer build-up. The samples were then dried in air at 70°C for 30 min and tested in 4-point bending (outer and inner span 40 and 20 mm, respectively) and flat support at room temperature for residual strength. This was calculated using maximum load before fracture according to the evaluation procedure prescribed in DIN 51110.[28]

3. Results

3.1. Microstructure, porosity and phase analyses

To facilitate a clear understanding of the relationship of the microstructure and the mechanical properties of this material, a brief summary of microstructural and phase development with heat treatment is given here. A comprehensive description is given in Ref. 20.

When the sprayed cylinder was observed optically in cross-section, rest lines or bands were evident, Fig. 2. These corresponded to the beginnings of the various sets of passes. However, they were very difficult to identify in SEM analyses. Generally, rest bands may be recognised in ceramographic sections as continuous bands of increased porosity and breakout of material during specimen preparation, but it is difficult to define their bounds. It was noticed, however, that on one edge of a rest band porosity increased abruptly, whereas on the opposite side it reduced gradually until no discernible difference to background porosity was identifiable. The quasi-layered splat structure and one edge of a rest band are clearly seen in the optical micrograph in Fig. 2. The rest bands and the quasi-layered splat structure were retained after all heat treatments. Inclusions of original α-Al_2O_3 powder agglomerates were also frequently observed within the microstructure.

The as-sprayed material was found to contain a mix of about 65% γ and γ-near transition phases and 35% α-Al_2O_3. The transition phases increasingly transformed to α-Al_2O_3 with progressively hotter heat treatment. Transformation was almost complete after the treatment at 1180°C. After heat treatment at 1550°C, the material was 100% α-Al_2O_3.

Archimedean porosity measurements, summarised in Fig. 3, show the overall porosity remains almost unchanged up to the reconstructive transformation to α-Al_2O_3. This transformation is accompanied by an increase in porosity of about 4%, despite it requiring a

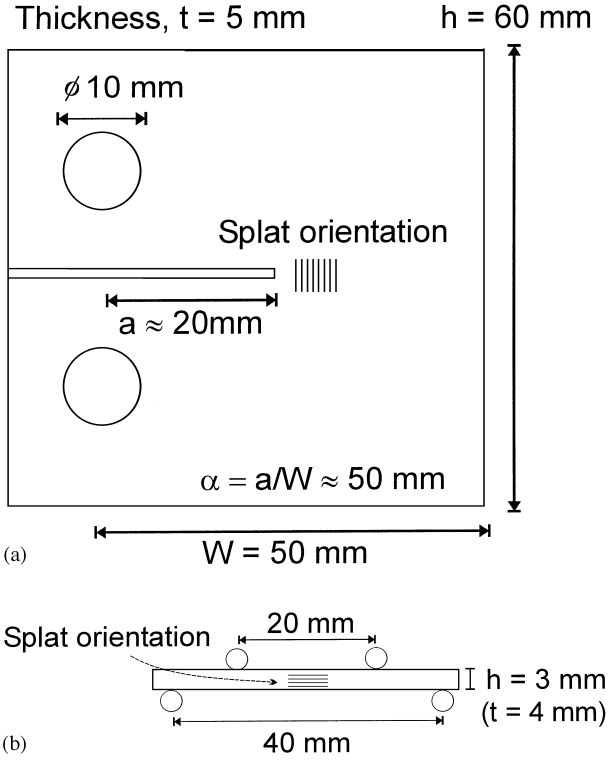

Fig. 1. Sample geometry and splat orientation: (a) CT sample for fracture toughness testing (a is effective notch length, W is effective sample width), and (b) a bending beam sample in a flat support.

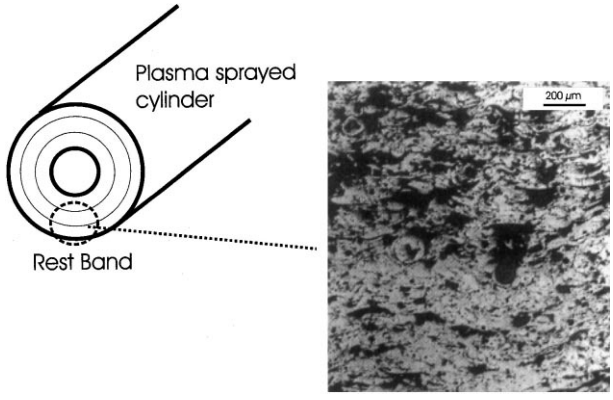

Fig. 2. Position and appearance of rest bands in a sprayed cylinder. The micrograph shows two distinct regions. In the upper part, material in a rest band can be seen. There is much more breakout indicating weaker cohesion that in the lower part, which shows neighbouring "normal" material.

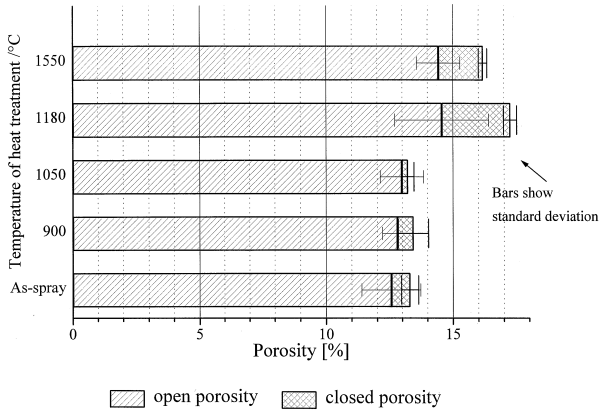

Fig. 3. Development of porosity with heat treatment.

consolidation of material. The heat treatment at 1550°C reduced porosity less than 1%, indicating little overall sintering had taken place.

The splats of the as-sprayed material had an internal columnar substructure, the columns being between 0.2 and 1 μm wide. An overview of splat substructures is given in the TEM micrograph in Fig. 4a. Cracking between columns can be seen. Selected area electron diffraction (SAED) showed that neighbouring columns have different crystallographic orientations. Agglomeration of porosity was observed at the columnar interfaces. Agglomeration of porosity and crystallographic mismatch may both contribute to weakening these interfaces. Generally, the as-sprayed material contains a high concentration of internal defects.

TEM observation of the microstructure after annealing at 900 and 1050°C for 12 h revealed no dramatic change from the as-sprayed condition. *Intra*-columnar porosity, however, became more pronounced, a feature not detected by porosimetry, probably because of the limited sensitivity of the Archimedean technique. This initial precipitation of porosity was most probably due to the condensation and rearrangement of quench defects out of the material as suggested in Refs. 29 and 30. These pores should not be confused with the microcrack formation sometimes observed on annealing due to the thermal expansion mismatch between neighbouring columns and splats. Such cracking leads to increased *inter*-columnar and inter-splat porosity — in fact, due to the TEM preparation techniques applied it is not possible to distinguish such thermal mismatch cracking from sample preparation damage.

Twelve hours at 1180°C allowed the material to transform almost completely to α-Al_2O_3. The columnar splat-substructure typical of the as-sprayed material had been replaced by a structure of self accommodating laths, Fig. 4b. The amount of porosity also visibly increased. The new laths, however, were reminiscent of the original columnar substructure. Numerous dislocations were identified and some formed dense networks. The splats were beginning a recovery process.

After 12 h at 1550°C the material was entirely α-Al_2O_3. The splat internal columnar and lath-like substructures had been completely replaced by small, slightly elongated grains. However, macroscopically, the basic quasi-laminated splat structure still prevailed. Fig. 4c shows the typical polycrystalline internal composition of a splat. Porosimetry showed porosity to be only slightly less than in the material after 12 h at 1180°C, indicating a small degree of sintering. Essentially, on a microscale this material was very similar to other sintered high alumina materials. Internally, the splats had undergone recrystallisation.

3.2. Fracture characteristics

The crack resistance of the samples was evaluated from the applied load and corresponding crack length according to ASTM standard E 399.[27] However, in the majority of cases, the crack projection method[31] had to be applied, as the cracks tended to quickly veer away from the plane of the notch. This method provides a conservative estimate of the fracture toughness and is valid if the deviation of the crack is not excessive. In cases where the deviation was greater than 35° no calculation of the fracture toughness was made. A summary of the results is presented in Fig. 5. For simplicity, values from different samples having undergone the

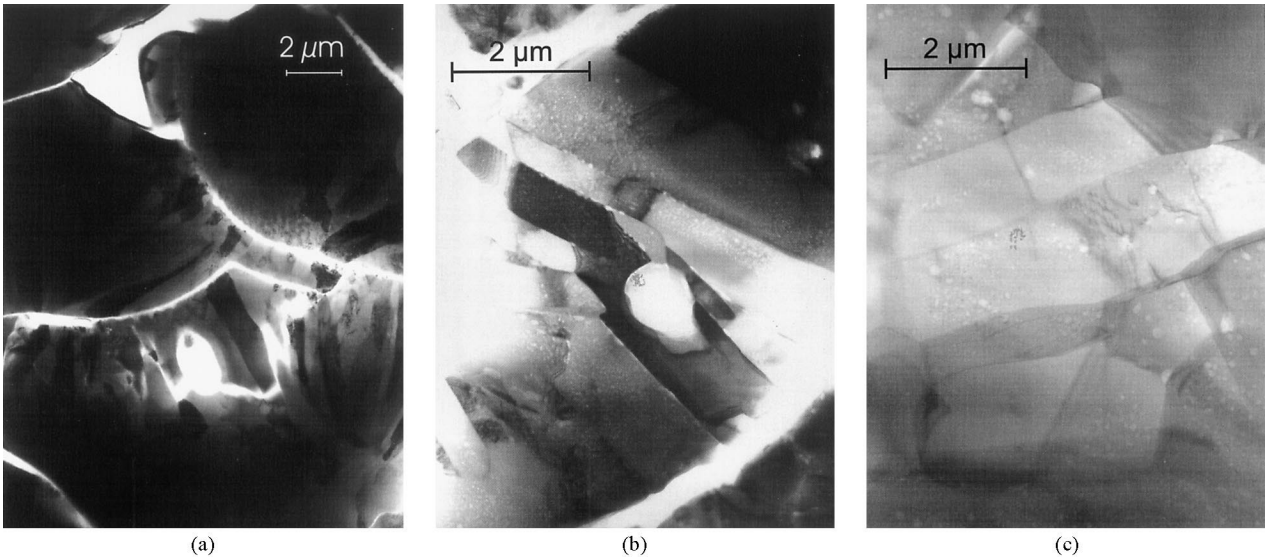

Fig. 4. TEM micrographs of internal substructure of splats: (a) columnar structure of as-sprayed splats, (b) lath structure after transformation to α-Al_2O_3 at 1180°C, (c) recrystallised grains within one splat after heat treatment at 1550°C for 12 h.

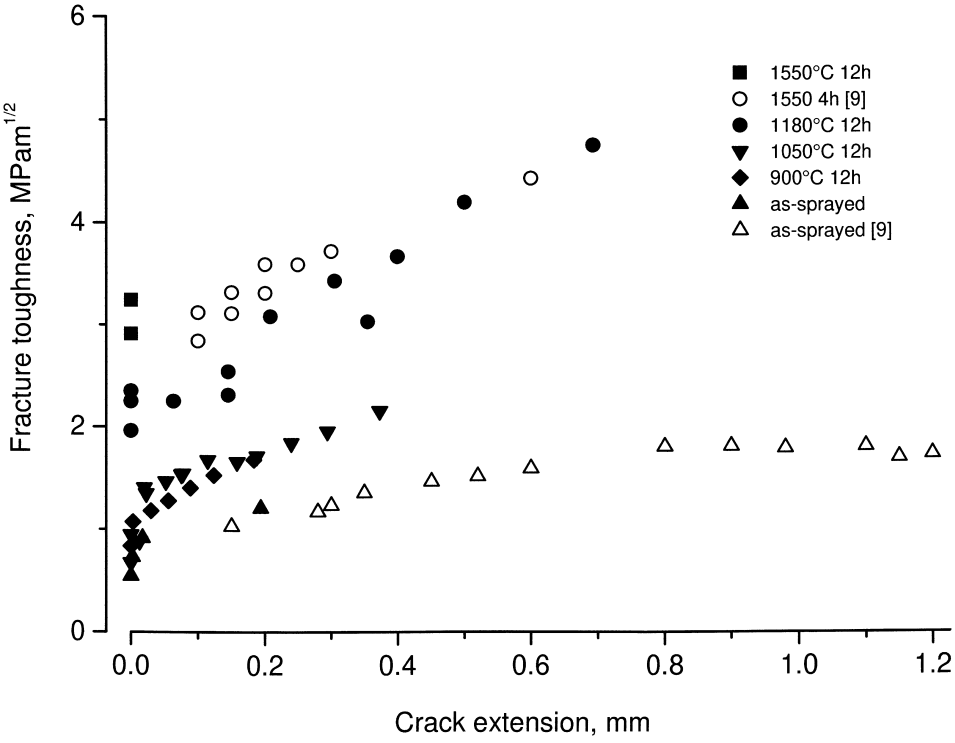

Fig. 5. Change in fracture toughness with crack extension. Open symbols refer to data from previous investigation on similar material.

same heat treatment are given the same symbols. In Fig. 5, results from a previous investigation [9] are also presented as open symbols. Although it is thought that factors such as specimen size and varying pre-notch depths can affect the absolute crack resistance determined,[32,33] the experimental conditions applied in this study were deemed similar enough to those in Ref. 9 to allow comparison.

The material exhibited pronounced *R*-curve behaviour in all conditions where extended controlled crack advance was achieved. In materials before the reconstructive transformation the fracture toughness rises sharply in the initial phase of crack advance, i.e. in the short crack range (within about 30–40 μm of crack growth), and then continues in the long crack range to rise at a much lower rate towards a plateau value. The initial toughness of the as-sprayed material is about 0.55 MPa $m^{1/2}$ and rises to a plateau of about 1.2 MPa $m^{1/2}$. The fracture surface of a splat in the as-sprayed condition is shown in Fig. 6a. The columnar internal structure is clearly recognisable.

After the heat treatments at 900 and 1050°C fracture toughness increases sharply. However, the main increase in toughening takes place in the early regime of crack growth. The rate of increase in toughness is higher for the material heat treated at 1050°C than for the material heat treated at 900°C. Both material conditions exhibit similar long crack fracture toughness at between 1.5 and 2 times that of the as-sprayed material. It is interesting to note that the rate of increase of fracture toughness is similar for as-sprayed material and heat treated materials in the long crack range.

After the phase transformation to α-Al_2O_3 at 1180°C the initial toughness jumped to around 2.3 MPa $m^{1/2}$. The fracture surface shown in Fig. 6b shows clearly just how similar the lath substructure of splats in this material is to the foregoing columnar substructure of the as-sprayed material. The toughness increased with crack extension at a higher rate than in the long crack range of materials before transformation. A corresponding short crack range could not be identified. The longest stable crack extension in this study was achieved on material in this condition. The highest valid toughness recorded was about 4.75 MPa $m^{1/2}$, an increase of about 100% on the initial value of this material and about 8.8 times higher than the initial fracture toughness of the as-sprayed material.

In the two samples heat treated at 1550°C for 12 h the crack advanced immediately after initation perpendicular to the plane of the notch and the specimens failed by intersplat delamination. Thus only an initiation fracture toughness can given at around 3–3.2 MPa $m^{1/2}$. This was up to 45% higher than that of material heat treated at 1180°C, and almost 6 times the initial fracture toughness of as-sprayed material. The fracture surface of a splat after heat treatment at 1550°C for 12 h is shown in Fig. 6c. Equiaxed or slightly elongated grains are dominant indicating recrystallisation.

Stable, straight crack propagation was achieved in all materials except that treated at 1550°C for 12 h. It was frequently observed that the crack deflected at or around included not completely melted powder particles. Crack deflection was more pronounced in heat treated materials. In all materials heat treated at less than 1550°C cracks tended to deviate eventually at about 30–35° to the plane of the notch and final failure usually occurred by sudden delamination. Post-fracture examination revealed this frequency occurred along rest bands. Occasionally, delamination perpendicular to the plane of the notch was seen to start even before the crack front had reached the rest band, see Fig. 7.

Achieving straight crack growth became progressively more difficult with increasing temperature of heat treatment. The amount of crack deflection and splitting was also seen to increase. Post-fracture examination of the fracture surfaces revealed a cog-tooth topography in the vicinity of the notch tip, typical of neighbouring splats which have broken across their thickness in different planes and have been pulled away from each other. The amount of delamination increased as the crack progressed. In the case of the tests made on material heat treated at 1550°C, the fracture surface showed virtually no sign of crack advance through splats. In general, the main toughening mechanisms observed operating were crack flank bridging, crack hinging, crack deflection

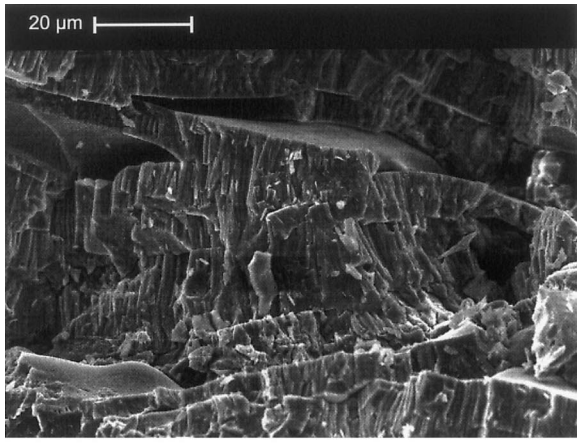

(a)

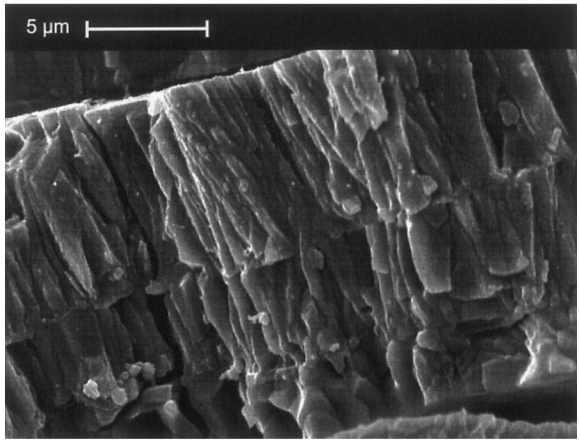

(b)

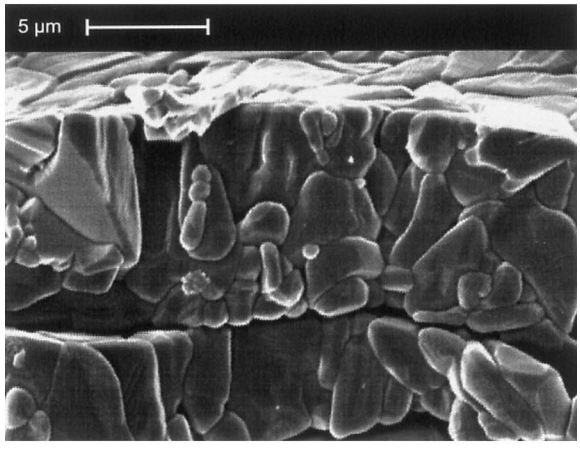

(c)

Fig. 6. Fracture surfaces of splats in (a) as-sprayed material, (b) after annealing at 1180°C for 12 h, and (c) in recrystallised material after heat treatment for 12 h at 1550°C. The micrograph in (a) is at a lower magnification to allow better visualisation of the splat layering and general fracture surface.

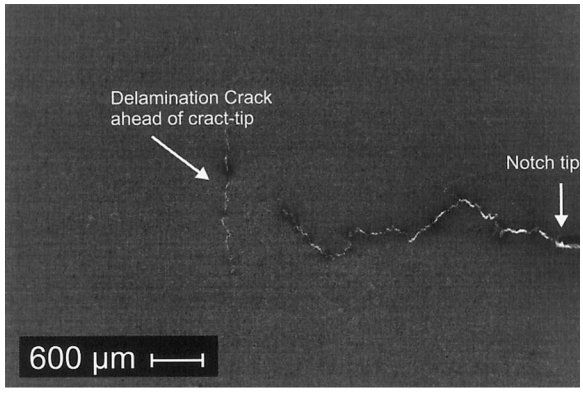

(a)

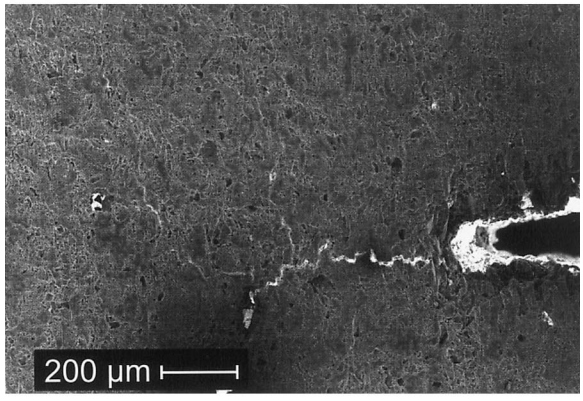

(b)

Fig. 7. (a) Overview of typical crack path, also showing delamination begining ahead of crack tip; and (b) higher magnification of typical crack path in short crack range: cog-tooth appearance of broken splats acting as bridging ligaments.

and crack splitting. A typical fracture path is shown in Fig. 7.

A slight load relaxation was also seen to occur during extended hold times during loading, e.g. in order to conduct crack length measurements. Such rest periods were subsequently kept as short as possible to minimise this effect.

3.3. Thermoshock

The results of strength and thermoshock tests are shown in Fig. 8. The as-sprayed material has a strength of about 22 MPa. A small increase in the strength of the material may be associated with the 900 and 1050°C heat treatments. Surprisingly, the strength of these three materials does not deteriorate after even a hard thermoshock of 1200°C. The reconstructive phase changes to α-Al_2O_3, after heat treatment at 1180°C, however, is associated with an appreciable (about 100%) increase in strength. In this material the strength does not deteriorate for thermoshocks up to 300°C. Residual strength continuously deteriorates for thermoshocks harder than this and with increasingly severe thermoshock tends to the value of the as-sprayed material.

The material heat treated at 1550°C for 12 h has an initial strength almost 3 times as high as that of the as-sprayed material, but this drops rapidly after a thermoshock of between 100 and 200°C. The strength of this material also tends towards that of as-sprayed material with increasing thermoshock severity. The residual strength of all material conditions after a thermoshock of 1200°C is about the same as that of as-sprayed material. In no case was a sudden drop in residual strength observed.

Fig. 9 shows sections through the microstructures of as-sprayed material, material after heat treatment at 1550°C for 12 h, and this material after a thermoshock of 1200°C. The sections were prepared under the same conditions and are, therefore, comparable. The splats of the as-sprayed structure show very fine internal transversal cracking. This can be seen in Fig. 9a, which, to highlight the fine cracks, is at a much higher magnification than the other two micrographs. This cracking is not evident on material after the heat treatment (Fig. 9b), but reappears on the material after it has experienced hard thermoshock (Fig. 9c). However, after thermoshock the cracks are not as fine, nor as finely dispersed through the material, as in the as-sprayed material. Comparison of the micrographs also indicates that the cohesion between splats, especially fine splats, is also increased by heat treatment.

4. Discussion

4.1. Toughness and toughening

The in situ SEM technique used here for fracture toughness evaluation provided especially good resolution in the early stages of crack growth. The present results agree well with those of the previous investigation.[9]

Fracture toughness in the as-sprayed condition is substantially lower than that of a conventionally sintered

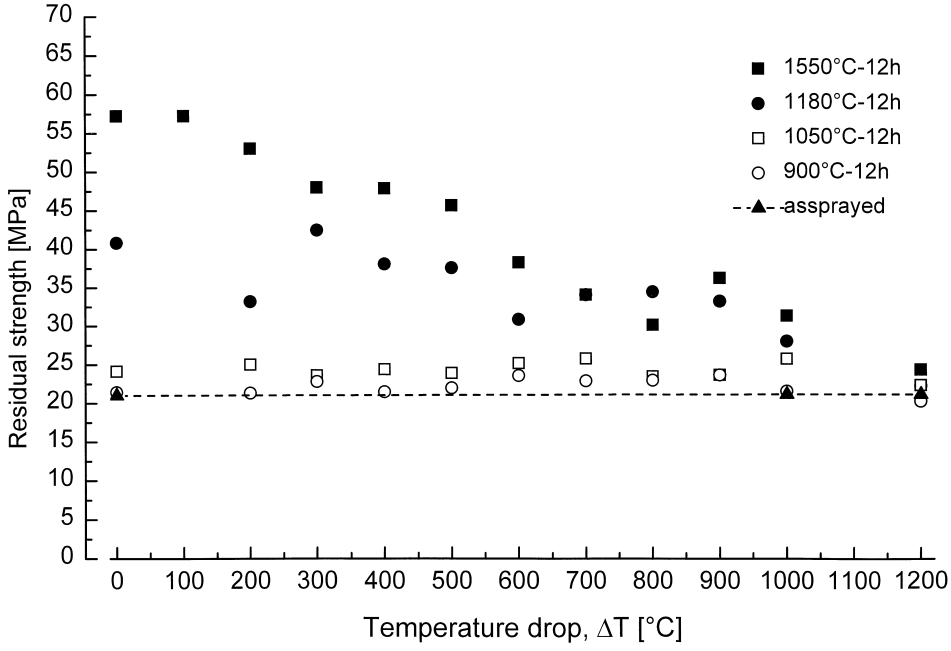

Fig. 8. Four point bending strength of material after different heat treatments, before and after thermoshock.

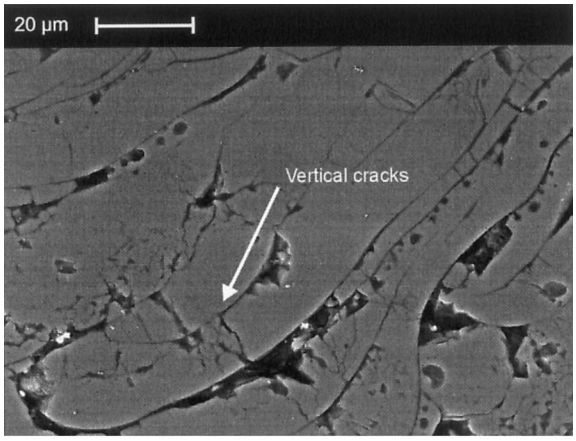

(a)

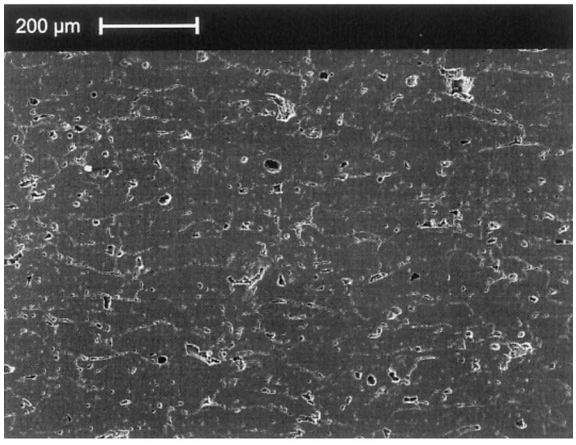

(b)

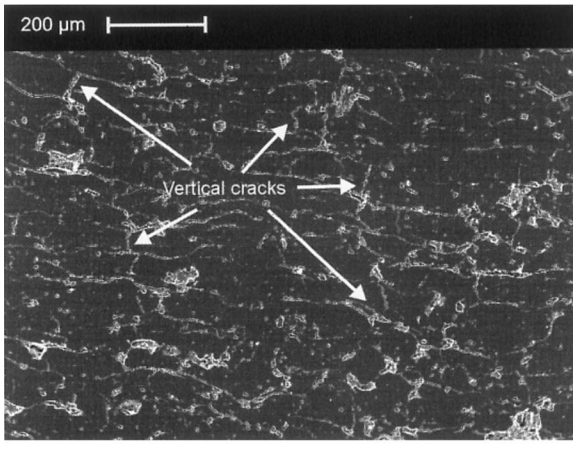

(c)

Fig. 9. Integrity of splats in (a) as-sprayed condition, (b) after heat treament at 1550°C for 12 h, and (c) after heat treatment at 1550°C for 12 h and thermoshock of $\Delta T = 1200°C$.

alumina. It is clear from Figs. 6a and 7 that in the as-sprayed condition the crack finds a path between columnar interfaces. TEM investigation has shown these to be areas of agglomerated porosity, crystallographic mismatch or other splat-transversal cracks and defects.[20] Healing of these defects or consolidation of this porosity with heat treatment first leads to an increase in the mechanical integrity of the splat making easy crack paths less accessible. Transformation to α-Al_2O_3 causes further consolidation of the microstructure by replacing columnar grains with interfacial mismatch by a system of self-accommodating laths. However, the boundaries between laths seem to offer a similar easy fracture path to the preceding columns. The resemblance of these new laths to the columnar grains before transformation may be seen from the fracture surface in Fig. 6b. A reduction in internal quench stresses must be concurrent with the consolidation of defects during morphological transformation. Both factors must be responsible for the jump in toughness and, as a consequence, in strength observed despite the transformation related increase in porosity.

Further annealing leads to an increase in intersplat cohesion and to the recrystallisation of the splat-internal structure, thereby making crack propagation through splats increasingly difficult. The increasing integrity of the splats may be readily inferred from the polycrystalline nature of the fracture surface of a splat after heat treatment at 1550°C, see Fig. 6c. Consequently, cracks are forced to greater deviation, despite the better cohesion of splats, and the toughness of the material improves and increases towards and above that expected of sintered, dense aluminas.

On observing crack initiation and advance, it was noticed that a crack tended to appear at a notch tip and advance through the first few splats in its path with relatively little deflection (Fig. 7b). It then began to deflect around large blocks of material and deviate away from the plane of the notch, typically at an angle of between 30 and 35°. It would then either be deflected further from, or back into the plane of the notch (Fig. 7a). Thus, there was clearly a transition between relatively straightforward crack advance in the short crack range, and the formation of large crack bridging ligaments in the long crack range. In the long crack range the crack also frequently underwent splitting and branching.

Since samples typically finally failed suddenly by delamination along intersplat interfaces in the rest bands, these are evidently the most mechanically weak regions in the material. This is supported by their appearance as areas of increased porosity after ceramographic sectioning. Their weakness may be explained if there is a lesser degree of bonding achieved between splats at the start of any spray procedure, when the substrate is cool, than after it is well under progress and the substrate has had time to warm up: warm substrates are well known to promote better adhesion.[34] Such a mechanism would explain why one edge of the rest band appears sharp and the other more diffuse. The rest bands identified are similar to the interlayer porosity described by Kudinov,[35] although the scale of the deposited layers is much larger in the present work.

The continuing crack advance even during periods when cross-head displacement was held constant implies that there is a certain inherent inertia in the fracture process and the material relaxes high stress concentrations by some time-dependent damage and deformation process. This is probably due to internal fracture of individual splats, the ligaments of which then slide over each other as the crack opening increases resulting in frictional redistribution of load. As a consequence, it is also likely that there is no clearly defined crack front, but rather a diffuse damage zone.

As seen in Fig. 5, toughness increases in the short crack range at a rate higher than 10 MPa $m^{1/2}$/mm, whereas in the long crack range it increases at a rate of $(1...4)\times10^{-3}$ MPa $m^{1/2}$/mm, which is four orders of magnitude lower, as schematically shown in Fig. 10. Thus, it is clear that different toughening mechanisms must dominate in each crack range.

In the short crack range the crack advances by breaking through splats (i.e. the crack advances perpendicular to the plans of the splats) and the initial toughening increment is a consequence of the mechanical interlocking and pull out of broken splats from their sockets. This leads directly to the typical cog-tooth fracture topography, an example of which is seen clearly in Fig. 6b. Thus the longer the segment that has to be pulled out, the greater the toughening increment per splat. The low toughness and toughening of the as-sprayed material may be explained by the fact that cracks can easily advance through splats by using the many low energy paths provided by the interfaces between neighbouring intra-splat columns and pre-existing transversal cracks due to residual thermal stresses. Thus the segments of splats pulled out are correspondingly short. It follows that, any reduction in the number of weak crack paths available, i.e. improvement in the integrity of individual splats, will result in longer segments being pulled out and, therefore, in a significant increase in toughness in this short crack range. This is what is observed in the material heat treated at 900 and 1050°C. Toughness continues to increase rapidly until an equilibrium condition is reached. As seen from Fig. 5 this occurs after 30 to 40 μm of crack advance.

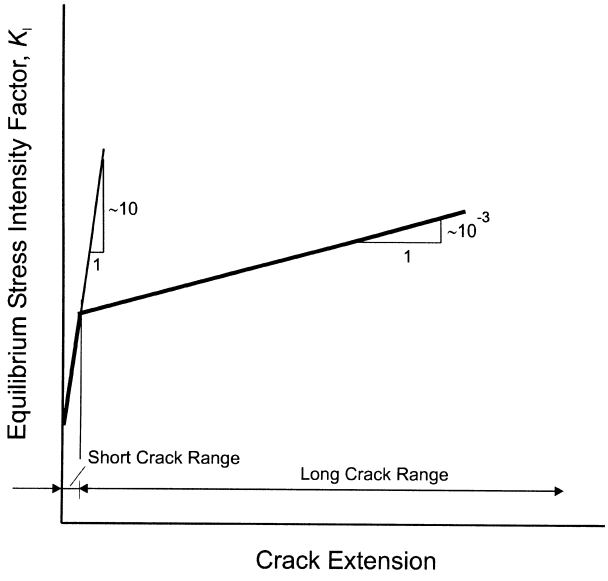

Fig. 10. Schematic representation of the short and long crack ranges of crack growth in as-sprayed material and material heat treated at 900 and 1050°C.

In order to understand the fracture behaviour better, it is instructive to consider a simple, qualitative model, which takes into account the effects of the peculiar cog-tooth-like pull-out of broken splats—see Appendix. (Several related models for conventional and fibre reinforced materials may be found in literature, see e.g. Refs. 36 and 37–40.) Applying this model shows that if the shearing stress between splats does not change after heat treatment at 900 and 1050°C, an increase of only 60% in fibre pull-out length is required to achieve the magnitude of toughening seen in these materials in the short crack range. This would, for example, correspond to a change in pull-out length from 10 to 16 μm and is in the range of pull-out lengths observed, see e.g. Fig. 7b.

After the crack has advanced sufficiently, other mechanisms of toughening can take effect: the crack may be forced to deflect around localised areas of better mechanical stability, or be offered easier paths by areas of relative weakness, resulting in crack splitting and an increase in fracture area; or, large blocks of material which have been circumvented by the advancing crack may act as elastic hinges between crack flanks and even impede crack opening by direct mechanical locking. Indeed, these mechanisms have all been observed in situ. They all have a long range effect as they require a larger scale of microstructural feature to operate. Presumably they would also reach an equilibrium condition after sufficient crack growth, and the toughness would exhibit a plateau value. Increasing microstructural integrity should result in larger blocks of material being circumvented or acting as ligaments and consequently a more tortuous crack path. Thus a greater toughening increment would be expected. Since, however, the heat treatments do not induce dramatic changes in the material at this scale of microstructure, the long range effect should be similar in all material conditions.

A combination of the mechanisms operating in the short and long ranges would explain the difference in initial toughness and toughening rates between the as-sprayed material and material heat treated at 900 and 1050°C, and the similarities in the rates of toughening in the long crack range of all materials.

4.2. Strength and thermoshock resistance

The strength of the plasma sprayed alumina improves considerably with heat treatment. This could be due to

two effects: an increase in contact area between splats due to sintering, or simply the rise in fracture toughness. For the first of these mechanisms to have effected the observed doubling and tripling in strength, the contact area between splats, given typically in literature as between 20 and 30% Refs. 41–43 would have had to increase very considerably and visibly. Since, however, only the material heat treated at 1550°C for 12 h showed noticeable improvement in inter-splat cohesion on microstructural examination, and given that porosity generally increased with heat treatments up to 1180°C, and was reduced only a little by the 1550°C heat treatment, it is felt that the improvement in cohesion between splats was generally not great enough to explain the observed increases in strength, and is probably a secondary and supplementary effect. The second strength increasing mechanism, characteristic of densely sintered brittle ceramic materials, only requires strength to scale proportionally with toughness. Exactly such behaviour was observed. Hence, it may be inferred that the strength of this plasma-sprayed alumina is really controlled by its fracture toughness. It then also follows that the changes in strength after heat treatment are a consequence of the same mechanisms that result in increased fracture toughness, i.e. the consolidation of defects during heat treatment, especially between intra-splat columnar grains. This mechanism is effective in materials heat treated at 900 and 1050°C, and even is more pronounced in material heat treated at 1180°C, in which the normal columnar substructure has been replaced by a system of self accommodating laths, and is even further accentuated by recrystallisation (and perhaps a little sintering) after 12 h at 1550°C.

The discussed increase in strength and toughness of this plasma-sprayed alumina notwithstanding, the ability of the material to withstand sudden temperature change without deterioration in its mechanical properties, i.e. its thermoshock resistance, is reduced with progressive heat treatment. However, the increase in strength with heat treatment was so great that even after experiencing maximum thermoshock the numerical value of residual strength of heat treated plasma-sprayed alumina always remained higher than, or equal to, the strength of as-sprayed material. Since no abrupt drop in strength after a thermoshock was observed in any material condition, it may be inferred that the material is always in the long crack regime of thermoshock behaviour.[44–46] Again this supports the idea that the effect of macroscopic splat sintering was small.

The fall in strength after hard thermoshock may be attributed to the reintroduction of weak paths for crack advance. This can be seen by the development of splat-internal cracking as shown in Fig. 9. The as-sprayed material has fine internal transversal cracks which probably either pre-existed or arose along weak columnar interfaces during polishing. Such cracks are far less common in the heat treated and recrystallised material. Transversal cracking then re-appears in material after it has experienced hard thermoshock probably as a result of thermal (quench) stresses. Hence, it is clear that it is the reintroduction of this splat-internal defect structure, despite its having a different origin from the as-sprayed defect structure, that is responsible for the reduction in strength after thermoshock. That the residual strength of heat treated material did not drop below the strength of as-sprayed material, supports this postulation.

The observations of this work are in broad agreement with the results of previous thermoshock investigations on similar materials. Lutz[5] for instance conducted strength and thermoshock tests on cylindrical specimens in both as-sprayed and annealed conditions including a bulk sprayed alumina. Nevertheless, there are some points of divergence. Although the initial strengths were found to be similar, Lutz found that even the "post-sintered" material was insensitive to sudden changes in temperature of up to 800°C, whereas in the present study deterioration in strength is observed at much lower thermoshocks. Furthermore, in his study, it was found that the strength of the post sintered and thermoshocked material could decrease to below the initial strength of the as-sprayed material. The differences in the results may stem from two primary sources: (1) the test configuration applied in Ref. 5 was considerably different (ring between plates) to that applied in the present work, (2) plasma-sprayed materials are like sintered ceramic materials, also susceptible to a size (geometry) effect in their thermoshock resistance.[46,47] This latter effect, in particular, makes comparison of absolute results between different sample geometries and experimental conditions difficult. However, in interpreting his results Lutz, in agreement with the present work, analogously concluded that thermoshock resulted in the formation of a microcrack network in plasma-sprayed ceramics and this was responsible for the deterioration in strength.

It should be noted that in the case of the material heat treated at 1180°C for 12 h the sample size chosen according according to DIN for strength and thermoshock testing may have been too small to allow the full applicability of linear elastic fracture mechanics (LEFM). In the worst case, if full toughness was achieved before fracture, then according to LEFM the critical crack must have been longer than sample height. However, in all other cases the critical crack would have been within the relevant sample dimension.

4.3. To summarise

It is suggested that the biggest and most significant change effected by heat treatment is the healing and removal, from within the splats, of microstructural easy

crack paths which result from rapid cooling processes during deposition. The increase in splat integrity results in large increases in both strength and toughness. This may be aided by the relaxation of internal stresses which must accompany the morphological rearrangement undergone during the transformation of transition phases to α-Al_2O_3. Heat treatment at temperatures close to standard sintering temperatures improves inter-splat cohesion, but this has a supplementary rather than a dominating effect on mechanical properties. Thermoshock can reintroduce splat internal defects, thereby facilitating crack propagation and causing a reduction in strength. The strength of all material conditions does not deteriorate to less than that of the as-sprayed material for any sudden temperature changes of up to 1200°C.

5. Synopsis and conclusions

Bulk plasma sprayed alumina has excellent thermoshock properties and can have good toughness and strength characteristics. Both fracture and strength behaviour can be significantly improved by heat treatment. However, the ability to withstand sudden temperature variation without change in mechanical properties is impaired.

In the as-sprayed condition splats of plasma sprayed aluminium oxide have a well developed substructure of γ-Al_2O_3 or α-Al_2O_3 columnar grains. The weak interfaces between the columns and other substructural defects provide low energy paths for crack advance and are largely responsible for the low toughness and low strength of the as-sprayed material. These defects, however, also contribute to the excellent thermoshock resistance of the material.

Annealing at 900 and 1050°C for 12 h does not significantly change the microstructure or mechanical behaviour of plasma sprayed alumina.

Heat treatment at 1180°C for 12 h results in replacement of the columnar substructure by a system of self-accommodating laths. The interfaces between laths still provide relatively weak, low energy preferential crack paths. The increase in integrity of the splat internal structure enhances toughening mechanisms and results in excellent toughness.

After 12 h at 1550°C the splats are internally completely recrystallised, but the macroscopic splat structure is largely retained. The intersplat cohesion is a little improved due to some sintering. Nevertheless, the material in this condition preferentially fails by delamination. This is mostly a consequence of the improved mechanical stability associated with recrystallisation of the splats, which makes crack advance through splats more difficult than crack deviation and propagation between splats.

All the material conditions (with the exception of material heat treated at 1550°C for 12 h, for which no controlled crack extension was achieved) exhibit pronounced *R*-curve behaviour. The *R*-curves may be divided into two regions: very steep in the initial phase of crack propagation, and flatter, but persistent, in the long range. In the short crack range toughening is a consequence of the pull-out of splats; and in the long crack range, the toughening effect results from crack branching and hinging by larger microstructural features.

The strength of plasma sprayed alumina is related directly to its fracture toughness. The considerable improvement in strength that accompanies heat treatment is a consequence of the improvement in toughness and the enhancement of toughening mechanisms. Sintering between splats has a supplementary, but not dominating effect.

As-sprayed Al_2O_3 has excellent thermoshock resistance and can withstand sudden temperature changes up to 1200°C, without suffering reduction in strength. The drop in strength after thermoshock is a result of the reintroduction of weak crack paths by thermal splat cracking.

An additional and important source of mechanical weakness in this bulk plasma sprayed ceramic are the rest bands which form in consequence of the cooling periods between the multiple sets of passes required to build up a thick deposit. These rest bands are areas of reduced splat cohesion and often dominate final failure.

Acknowledgements

This work was funded in part by the Austrian Ministry for Science and Transport under the contract no. GZ 140.539/3-V/A/6/98.

Appendix. A mechanistic model of toughening by splat pull-out

Since crack advance in plasma-sprayed ceramics results in a typical and unique cog-tooth fracture topography, see Fig. 6b, a frictional energy dissipation approach, based on the Kelly–Tyson model for strength behaviour in fibre reinforced metal matrix composites, assuming a linear transfer of load into a splat by friction at its interface with neighbouring splats,[37–40] can be used to estimate the contribution to toughening by splat pull-out.

The initial toughness, G_{Ic}, determined by twice the fracture energy of splats per unit crack area γ_f is increased by the total work of splat pull-out per unit area of projected crack surface, W_{tot}, so that the final toughness is given by

$$G_R \equiv G_{Ic} + \Delta G = 2\gamma_f + W_{tot}. \quad (A1)$$

In the range of validity of linear elastic fracture mechanics, initial and final toughness are related to the corresponding critical equilibrium stress intensity factors and elastic modulus E by [48]

$$G_{Ic} = \frac{K_{Ic}^2}{E} \text{ and } G_R = \frac{K_R^2}{E}, \quad (A2)$$

so that the increase in toughness, or the work of pull-out per unit area, is given by

$$\Delta G \equiv W_{tot} = \frac{K_R^2 - K_{Ic}^2}{E}. \quad (A3)$$

A splat of plasma-sprayed material can be idealized as a thin rectangular plate of which w and thickness t, Fig. A1. Each alternate splat in the stacking direction may be regarded as being locked into a matrix formed by its neighbouring splats. Thus, as a crack advances in this direction, and opens, every second splat may be assumed to be pulled-out of its matrix, analogously to short fibre reinforcements in ceramic matrix composites. The toughening increment results from the frictional energy dissipated during pull-out. The work of pull-out can be estimated by considering the equilibrium between tensile and sliding fractional forces acting on one splat. By regarding a splat segment of infinitesimal height dx, and assuming that the interfacial shear stress remains constant, then

$$(\sigma + d\sigma)\cdot wt = \sigma\cdot wt + \tau_i\cdot 2(w+t)\cdot dx, \quad (A4)$$

where σ is the stress normal to the segment and τ_i is frictional force per unit surface area, i.e. interfacial shear stress.

It follows from Eq. (A4) that

$$\frac{d\sigma}{dx} = \frac{2\tau_i(w+t)}{wt}, \quad (A5)$$

and the normal stress acting at a distance x from the base of the extruding splat is

$$\sigma = \int_0^x \frac{2\tau_i(w+t)}{wt}dx = \frac{2\tau_i(w+t)}{wt}.x. \quad (A6)$$

This linear relationship is shown in Fig. A1b. Since the rate of work is given by

$$\frac{dW}{dx} = F, \quad (A7)$$

where F is force, the work done on pulling out one splat an entire pull-out length l is

$$W_s = \int_0^l \sigma\cdot(wt)\cdot dx = \int_0^l 2\tau_i(w+t)x dx = \tau_i(w+t)l^2. \quad (A8)$$

Assuming all splats are equal, and since according to the model only every second splat is pulled out of its matrix, the number of effective splats per unit area is given by

$$n = \frac{1}{2wt}. \quad (A9)$$

Thus the total work of pull-out done per unit area of crack surface is

$$W_{tot} = \frac{\tau_i(w+t)l^2}{2wt}. \quad (A10)$$

The final formula for toughening by frictional energy dissipation in plasma-sprayed ceramics can be obtained by combining and rearranging Eqs. (A3) and (A10) as

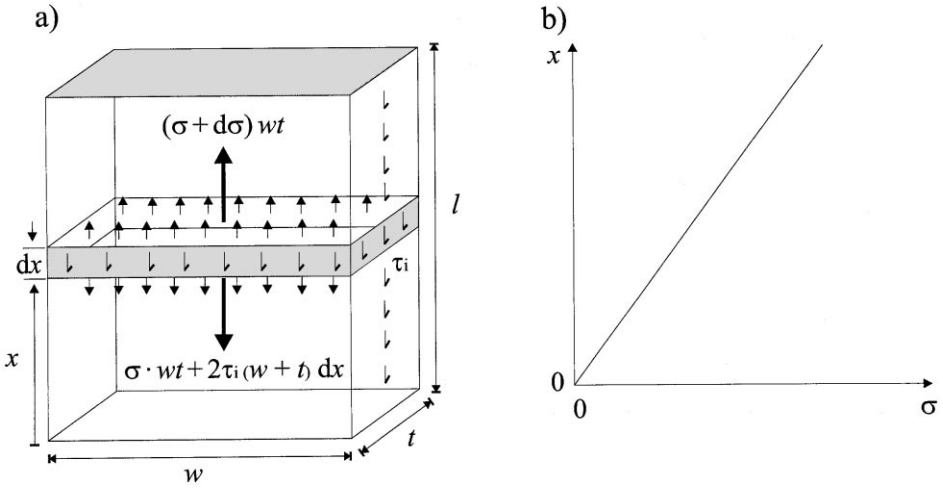

Fig A1. (a) Schematic representation of idealized splat and forces acting on a segment, (b) Linear dependance of normal stress (i.e. load transfer) with distance x.

$$\tau_i \cdot l^2 = \frac{2(K_R^2 - K_{Ic}^2)}{E} \cdot \frac{wt}{w+t}. \quad \text{(A11)}$$

It can be seen that the two parameters important for achieving toughening are average length of pull-out and interfacial shear stress.

Example

From microstructural studies, the average splat in the as-sprayed state may be assumed to have thickness $t = 10$ μm, and width $w = 100$ μm.[9] Preliminary studies have indicated that this material has an elastic modulus of around E = 60 GPa in the direction perpendicular to splat stacking,[49] i.e. normal to the plane of cracks being considered.

If a pull-out length of 10 μm is assumed in the as-sprayed material (as seen approximately in SEM analysis), and taking K_{Ic} and K_R values from experimental results, see Fig. 5, the interfacial shear stress may be estimated from Eq. (A11) as $\tau_i = 2.3$ MPa. This is a very reasonable value for physically bonded interfaces and is of the same order of magnitude as values of interfacial shear stress measured in various composite materials.[50–53]

Furthermore, if it is assumed that the interfacial shear strength does not change much or at all by heat treatments at temperatures below the temperature of phase change to α-alumina, the toughening increment observed in the material heat treated at 1050°C for 12 h could be achieved by increasing the length of pull out to about 16 μm. This is also a very reasonable figure close to the values observed (cf. SEM micrograph of short crack regime in Fig. 8b).

The above estimations both support the postulation that splat pull-out is largely responsible for the toughening observed in material heat treated at relatively low temperature.

References

1. Pawlowski, L., *The Science and Engineering of Thermal Spray Coatings*. Wiley, Chichester, 1995.
2. Heimann, R., *Plasma-Spray Coating: Princiles and Applications*. VCH, Weinheim-New York, 1996.
3. Smith, R.W. Plasma Spray Processing... the state of the art... and future — from a surface to a materials processing technology. In: 2nd Plasma-Technik-Symp., Vol. 1, Lucerne. Wohlen, Switzerland, 1991, pp. 17–38.
4. Lutz, E. H., Plasma spraying of ceramics — an alternative to conventional production of components. *Interceram*, 1993, **42**, 160.
5. Lutz, E. H., Plasma ceramic. *Powder Metallurgy International*, 1993, **25**, 131–137.
6. Lutz, E. H., Crack resistance anisotropy in plasma-sprayed ceramic composites. *Fach-berichte der DKG*, 1995, **72**, 713–716.
7. Lutz, E. H., Microstructure and properties of plasma ceramics. *J. Am. Ceram. Soc*., 1994, **77**, 1274–1280.
8. Lutz, E. H., The effect of specimen size on the thermal shock resistance of plasma-sprayed ceramics. *Facherichte der DKG*, 1995, **72**, 387–389.
9. Damani, R. J. and Lutz, E. H., Microstructure, strength and fracture characteristics of a free standing plasma-sprayed alumina. *J. Eur. Ceram. Soc*., 1997, **17**, 1351–1359.
10. Wanner, A. and Lutz, E. H., Elastic anisotropy of plasma-sprayed, free-standing ceramics. *J. Am. Ceram. Soc*., 1998, **81**, 2706–2708.
11. Wang, D. and Berndt, C. C., Anistropic thermal expansion behaviour of thermally sprayed coatings. In *2nd Plasma-Technik-Symp., Vol. 2, Lucerne*. Wohlen, Switzerland, 1991, pp. 295–304.
12. Steffens, H.-D. and Fischer, U., Correlation between microstructure physical properties of plasma sprayed zirconia coatings. In *Thermal Spray Technology — New Ideas and Processes*, ed. D. L. Houck. ASM International, Materials Park, 1988, pp. 167–173.
13. Eichhorn, F., Metzler, J. and Eysel, W., Röntgenbeugungsuntersuchungen an plasmage-sprizten Aluminiumoxidschichten. *Metalloberfläche Angew. Elektrochemie*, 1972, **26**, 212–213.
14. McPherson, R., Formation of metastable phases in flame and plasma-prepared alumina. *J. Mat. Sci*., 1973, **8**, 851–858.
15. McPherson, R., On the formation of thermally sprayed alumina coatings. *J. Mat. Sci*., 1980, **15**, 3141–3149.
16. Dauger, A., Fargeot, D. and Laval, J. P., Metastable phases of alumina. In *Mat. Res. Soc. Symp. Proc., Vol. 21*. Elsevier, Amsterdam, 1984, pp. 207–211.
17. Lutz, E. H., Plasma ceramics — properties and applications. *Fachberichte der DKG*, 1997, **74**, 148–151.
18. Thompson, V. S. and Whittemore, O. J. Jr., Structural changes on reheating plasma-sprayed alumina. *Cer. Bull*., 1968, **47**, 637–641.
19. Safai, S. and Herman, H. Plasma-sprayed materials. In *Treatise on Materials Science and Technology, Vol. 20*. Acadamic Press, New York, 1981, pp. 183–213.
20. Damani, R. J. and Makroczy, P., Heat treatment induced phase and microstructural development in bulk plasma sprayed alumina. *J. Eur. Ceram. Soc*., 2000, **20**(7), 867–888.
21. Glitzen, W., *Aluminia as a Ceramic Material*. Special Publ. No. 4, The American Ceramic Society, 1970.
22. Wefers, K. and Misra, C. *Oxides and Hydroxides of Aluminium*. Alcoa Techn. Paper No. 19, Revised, Alcoa Laboratories, 1987.
23. Morrell, R., *Handbook of Properties of Technical & Engineering ceramics, Part 2: Data Reviews, section 1: High-Alumina Ceramics*. HM Stationary Office, London, 1987.
24. Taschl, A., et al., Einsatz der Orientation Image Microscopy zur Charakterisierung von Ver-formungsvorgaengen: In *Sonderband der Praktischen Metallographic*, ed. A. Kneissl and F. Jeglitsch. Verlag Werkstoff-Informationgesellschaft, Frankfurt (in press).
25. Damani, R. J., Gstrein, R. and Danzer, R., Critical notch-root radius effect in SENB-S fracture toughness testing. *J. Eur. Ceram. Soc*., 1996, **16**, 695–702.
26. Damani, R. J., Schuster, Ch. and Danzer, R., Polished notch modification of SENB-S fracture toughness testing. *J. Eur. Ceram. Soc*., 1997, **17**, 1685–1689.
27. ASTM Standard E 399-83: Standard test method for plane-strain Fracture Toughness of Metallic Materials.
28. DIN 51110, Teil 1, Prüfung von keramischen Hochleistungdwerkstoffen, 4-Punkt-Biegever-such bei Raumtemperatur, Entwurf, February 1990.
29. Braue, W. et al., In-plane microstructure of plasma-sprayed Mg-Al Spinel and 2/1-mullite based protective coatings: an electron microscopy study. *J. Eur. Ceram. Soc*., 1996, **16**, 85–97.
30. Fargeot, D. et al., Elastic and anelastic effects associated with precipitation phenomena in non-stoichiometric spinels. *J. de. Physique*, 1981, **42**, 899–904.
31. Fischer, F. D. and Rammerstorfer, F. G., Evaluation of mode-I crack projecton procedures using the strain energy criterion. *Theor. Appl. Frac. Mech*., 994, **20**, 67–74.

32. Lutz, E. H. and Swain, M. V., Significance of the specimen size of the K_R-curve behavior of quasi-brittle materials. *J. Eur. Ceram. Soc.*, 1994, **13**, 501–507.
33. Lutz, E. H. and Sakai, M., R-Curve and compliance change upon renotching. *J. Am. Ceram. Soc.*, 1993, **76**, 3113–3122.
34. Longo, F. N., *Processing and design. A lesson from Thermal Spray Technology, Course 51*. Materials Engineering Institute, ASM International, Materials Park, OH, 1994.
35. Kudinov, V. V., Pekshev, P. Yu. and Safiullin, V. A., Forming of the structure of plasma-sprayed materials. In *High-Temperature Dust-Laden Jets in Plasma Technology*, ed. O. P. Solonenko and A. I. Fedorchenko. VSP, Utrecht, The Netherlands, 1990, pp. 381–418.
36. Steinbrech, R. W., Reichl, R. and Schaarwächter, W., R-Curve behaviour of long cracks in alumina. *J. Am. Ceram. Soc.*, 1990, **73**, 2009–2015.
37. Kelly, A. and Tyson, W. R., Tensile properties of fibre reinforced metals: copper/tungsten and copper/molybdenum. *J. Mech. Phys. Solids*, 1965, **13**, 329–350.
38. Kelly, A. and Tyson, W. R., Tensile properties of fibre reinforced metals — II. Creep of silver–tungsten. *J. Mech. Phys. Solids*, 1966, **14**, 177–186.
39. Ashby, M. F. and Jones, D. R. H., *Engineering Materials 2: An Introduction to Microstructures, Processing and Design*. Pergamon Press, Oxford, 1992.
40. Hull, D., *An Introduction to Composite Materials*. Cambridge University Press, Cambridge, 1992.
41. Arata, Y., Ohmori, A. and LI, C.-J., Electrochemical method to evaluate the connected porosity in ceramic coatings. *Thin Solid Films*, 1988, **156**, 315–325.
42. McPherson, R., Cheang, P., Microstructural analysis of Ni-Al plasma spayed coatings. In *Proceedings of the 12th Int Thermal Spraying Conf., London*, 1989, Paper 17.
43. McPherson, R. and Shafer, B. V., Interammellar contact within plasma-sprayed coatings. *Thin Solid Films*, 1982, **97**, 204–210.
44. Hasselman, D. P. H., Unified theory of thermoshock fracture initiation and crack propagation in brittle materials. *J. Am. Ceram. Soc.*, 1969, **52**, 600–604.
45. Gupta, T. K., Strength degredation and crack propagation in thermally shocked Al_2O_3. *J. Am. Ceram. Soc.*, 1972, **55**, 249–253.
46. Schneider, G. A., Danzer, R. and Petzow, G., Zum Thermoschockverhalten spröder Werkstoffe. *Fortschrittsberichte der DKG*, 1988, **3**, 59–70.
47. Magerl, F., *Thermoshock-und thermisches Ermüdungsverhalten von keramischen Werkstoffen unter bruchmechanischen Aspekten*. Düsseldorf, VDI-Verlag, 1994.
48. Davidge, R. W. and Van de Voorde, M. H., *Designing with Structural Ceramics*. Elsevier, London, 1991.
49. Wanner, A. and Damani, R. J., Effect on annealing on the microstructure and elastic properties of plasma-sprayed alumina. *10th Int. Conf. on Rapidly Quenched and Metastable Materials*, Indian Institute of Science, Bangalore, 1999, accepted.
50. Chou, H. M., Barsoum, M. W. and Koczak, M. J., Effect of temperature on tnterfacial shear strengths of SiC/glass interfaces. *J. Mat. Sci.*, 1991, **26**, 1216–1222.
51. Bright, J. D., Danchaivijit, S. and Shetty, D. K., Interfacial sliding friction in silicon carbide–borosilicate glass composites: a comparison of pullout and pushout tests. *J. Am. Ceram. Soc.*, 1991, **74**, 115–122.
52. Martin, B., Benoit, M. and Rouby, D., Interfacial sliding strength in fibre reinforced ceramic matrix composites involving positive radial thermal misfit strain. *Scipta Metal. et Mat.*, 1993, **28**, 1429–1433.
53. Weihs, T. P. and Nix, W. D., Experimental examination of the push-down technique for measuring the sliding resistance of silicon carbide fibers in a ceramic matrix. *J. Am. Ceram. Soc.*, 1991, **74**, 524–534.